BISTATIC SAS IMAGING STUDIES

SK Mitchell Applied Research Laboratories, The University of Texas at Austin, USA
KN Scarbrough Applied Research Laboratories, The University of Texas at Austin, USA
SP Pitt Applied Research Laboratories, The University of Texas at Austin, USA

1 INTRODUCTION

Future minehunting system concepts include multiple autonomous underwater vehicle operations allowing for the possibility of bistatic and/or multistatic sonar operations. Under sponsorship of the ONR Shallow Water Autonomous Mine Sensing Initiative (SWAMSI), the Applied Research Laboratories of the University of Texas at Austin (ARL:UT) is investigating bistatic synthetic aperture processing, and in particular bistatic circular SAS (CSAS) imaging.

In monostatic radar or sonar, with either conventional or synthetic aperture, only one basic concept of operation arises: the platform maneuvers to ensonify the target region and acquire echoes. With bistatic operation, where source and receiver platforms may move independently with respect to each other and the target region, several concepts may be specified, depending upon whether one or both platforms transmit or receive, how the platforms move, and where they are located with respect to the target region and to each other. Three possibilities are shown in Figure 1. In Figure 1A, a "mother" platform ensonifies the target region while a UUV encircles the region to acquire echoes. Analysis of bistatic data from the configuration of Figure 1A has been previously reported[1]. In Figure 1B, two UUV platforms traverse on parallel tracks; both ensonify the region between them and acquire echoes. In Figure 1C, ensonification is provided by one or more fixed sources within the target region; echoes are received by a UUV which encircles the region and the data are processed in a synthetic aperture fashion.

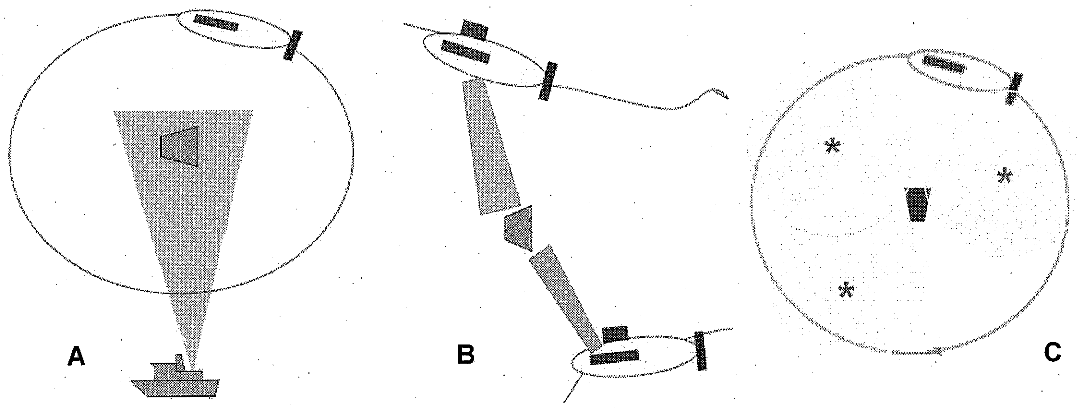

Figure 1. Bistatic SAS Configurations. A.. Source on mother platform, receiver on UUV.
B. Two UUV's traverse region, source/receiver on both UUV's.
C. Fixed sources in target region, receiver on UUV.

Section 2 of this paper provides an overview of the CSAS bistatic image processing algorithm along with example images generated from synthesized echo data. Examples of bistatic CSAS imaging with data from the configuration in Figure 1C are given in Sections 3 and 4. Section 3 presents imaging results for bistatic target echoes acquired from the Rotating Seabed facility of ARL:UT, while Section 4 presents the results of a trial with targets deployed on the bottom of Lake Travis, a single, fixed source in the target field, and a surface platform-mounted receiver. The facilities, targets, and data acquisition equipment described in Sections 3 and 4 were also used for the work reported in a companion paper that will appear in the proceedings of this conference[2].

2 BISTATIC SYNTHETIC APERTURE PROCESSING

Algorithms for image reconstruction from bistatic data are similar to monostatic algorithms just as bistatic echo formation is similar to monostatic echo formation. Figure 2 illustrates the computation for an echo from the target reflectivity function, $m(x,y)$, where the target bistatic aspect is ϕ and the bistatic angle is β. Source and receiver locations are usually known in terms of absolute coordinates, e.g., latitude and longitude, but to develop the image processing algorithms it is easier to express the geometry in terms of ϕ and β. We use the convention that, when β = 180°, the source, target, and receiver lie in that order on a line. The echo, $e(t)$, can be related to the transmitted pulse, $s(t)$, and the target reflectivity function, $m(x,y)$, by the integral expression of Equation (1) in Figure 2. From this expression, it is straightforward to show that the echo spectrum, $E(\omega)$, is given by the bistatic Fourier-Slice formula given by Equation (2) in Figure 2.

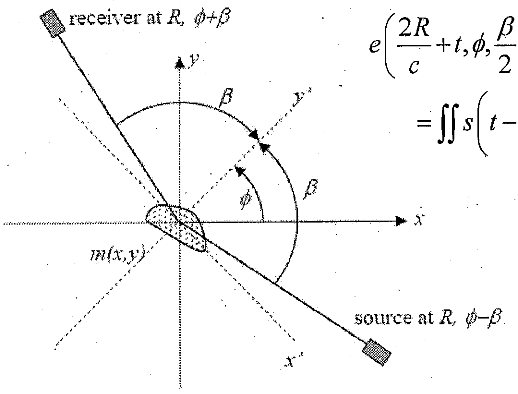

$$e\left(\frac{2R}{c}+t,\phi,\frac{\beta}{2}\right) = \iint s\left(t-\frac{2y'}{c}\cos\frac{\beta}{2}\right) m\left(y'\cos\phi+x'\sin\phi,\, y'\sin\phi-x'\cos\phi\right) dx'\,dy' \quad (1)$$

$$E(\omega,\phi,\beta) = S(\omega)\, M\left(\frac{2\omega}{c}\cos\frac{\beta}{2},\, \phi\right) \quad (2)$$

Figure 2. Bistatic Geometry, echo *e(t)* from target *m(x,y)*. Equation 2 is the bistatic form of the Fourier-Slice Theorem. $M(k_x,k_y)$ is the Fourier transform of $m(x,y)$.

Bistatic images can be generated from a direct Fourier reconstruction algorithm as follows:

- For each echo $e(t)$, determine ϕ and β from navigation data, compute spectrum $E(\omega)$ via FFT.
- Map $E(\omega)$ to rectangular wavenumber coordinates as $M\left(\frac{2\omega}{c}\cos\frac{\beta}{2}\cos\phi, \frac{2\omega}{c}\cos\frac{\beta}{2}\sin\phi\right)$.
- After all pings have been processed, compute the two dimensional Fourier transform of $M(k_x,k_y)$ to yield the reconstructed image, $m(x,y)$.

Figure 3 shows simulation results for 13 omnidirectional point reflectors distributed along an ellipse with semi-major and semi-minor axes of 1.0 m and 0.5 m, centered at the origin. Note that all reflectors are visible from all aspects (no shadowing). A fixed source transmits a Gaussian pulse centered at 30 kHz at 30° bearing; the source direction is shown by the yellow arrow in Figure 3. The receiver acquires 900 echoes as it moves around the target at a fixed rate and a fixed range. The bistatic sinogram, Figure 3A, shows that all of the echo components arrive simultaneously when the bistatic angle β is 180°. The direct blast arrival is not shown in these simulations. The wavenumber transformed data, $M(k_x,k_y)$, is shown in Figure 3B. Because of the bistatic reconstruction algorithm, it occupies only one-fourth of the wavenumber region. The crescent shape arises from the factor $\cos\beta/2$. The reconstructed image of the target reflectivity function, $m(x,y)$, in Figure 3C accurately reflects the location of the simulated point reflectors; the point spread in the reconstructed image is least in the direction downrange from the source, and greatest in the cross-range direction.

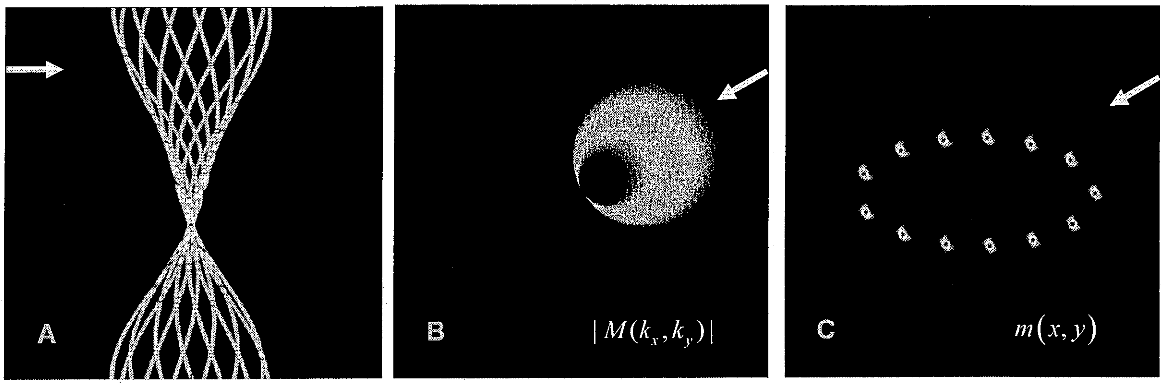

Figure 3. Bistatic simulation results for 13 point reflectors. Fixed source is at 30° bearing; indicated by arrow in each frame. A. Bistatic sinogram for 360° receiver orbit; ± 3 ms window. B. Echo data in wavenumber space. C. Reconstructed image.

Figure 4 shows the results of a second bistatic simulation for a solid, 20 cm x 50 cm, truncated ellipse target. A fixed source located at a bearing of 50° transmits a Gaussian pulse while the receiver circles the target. Laplacian shading was used so that echoes are received only from the exterior of the illuminated portion of the solid. The reconstructed image, Figure 4B, shows that the illuminated portion is clearly reproduced. For reference, the reconstructed image for a simulated monostatic data set (co-located source and receiver circling the target) is shown in Figure 4C.

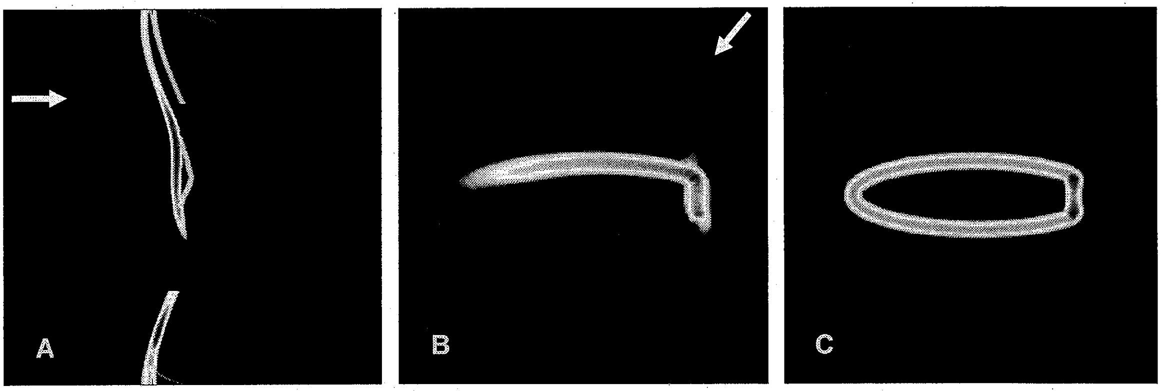

Figure 4. Bistatic simulation results for solid truncated ellipse. Fixed source is at 50° bearing. A. Bistatic sinogram for 360° receiver orbit; ± 1 ms window. B. Reconstructed bistatic image. C. Monostatic image for comparison

The analysis and simulated results of this section assume that both source and receiver are in the far field so that wavefront curvature effects need not be addressed. The same assumption is made implicitly in the image processing applied to the data sets in Sections 3 and 4, even though some of the source-target distances are rather short. As will be seen, the quality of the imaging results in Sections 3 and 4 suggests that bistatic wavefront curvature effects are not a significant issue at the distances considered in these data sets.

3 BISTATIC LABORATORY DATA

Bistatic echo data were acquired with the rotating seabed[2], a 6 m diameter sand-filled turntable, at the ARL:UT Lake Travis Test Station. The bistatic geometry is illustrated in Figure 5A. A small cylindrical projector (2.5 cm diameter, 2.5 cm high) was mounted 30 cm above the turntable, with the targets placed near the opposite edge. The transmit waveform was a 50-95 kHz LFM (linear frequency modulated) pulse. Echoes were received by a fixed sonar array 30 m away. Here the source rotates, along with the target region, while the receiver is fixed, which is equivalent to the bistatic configuration sketched in Figure 1C. The targets used in this trial were a wire lobster trap shown in Figure 5B, and an air-filled steel cylinder shown in Figure 5C.

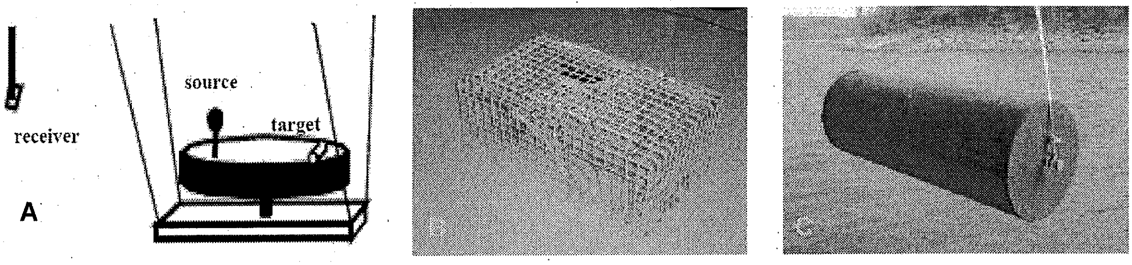

Figure 5. A. Bistatic turntable configuration. B. Lobster trap 120 cm x 45 cm x 45 cm. C. Steel cylinder, 30 cm diameter x 90 cm long.

Figure 6 compares monostatic and bistatic images from the lobster trap. Bistatic data were acquired for two orientations of the lobster trap relative to the source at 90° (indicated by yellow arrows), a near quarter aspect in Figure 6B, and a near beam aspect in Figure 6C. Similarly to the distributed point reflectors in the example of Figure 3, the wire trap is partially transparent. Portions of the trap other than the side closest to the source are also ensonified and reproduced in the bistatic images.

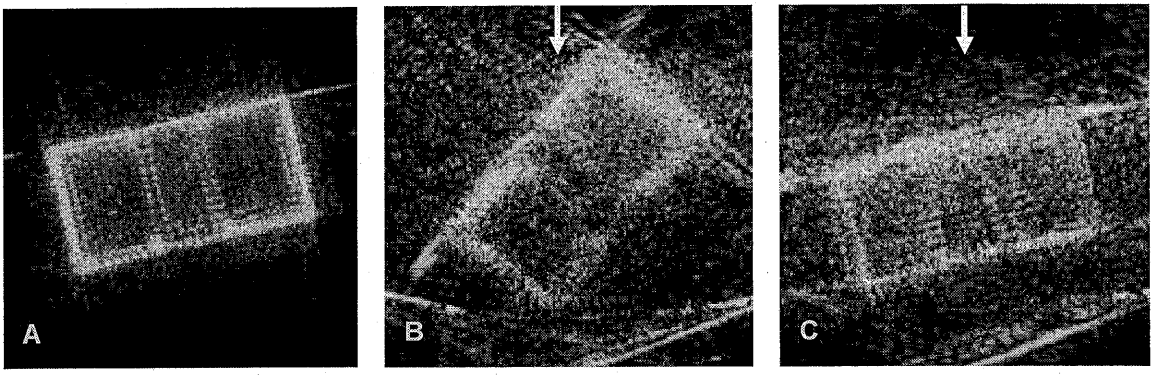

Figure 6. CSAS Images of lobster trap. A. Monostatic image. B. Bistatic image of lobster trap near quarter aspect. C. Bistatic image of lobster trap near beam aspect.

Figure 7 compares monostatic and bistatic images from the steel cylinder. As with the solid target simulation results in Figure 4, the portions of the target ensonified by the bistatic fixed source are imaged very well. At the bottom of Figure 7B, the cylinder is observed to shadow the turntable edge.

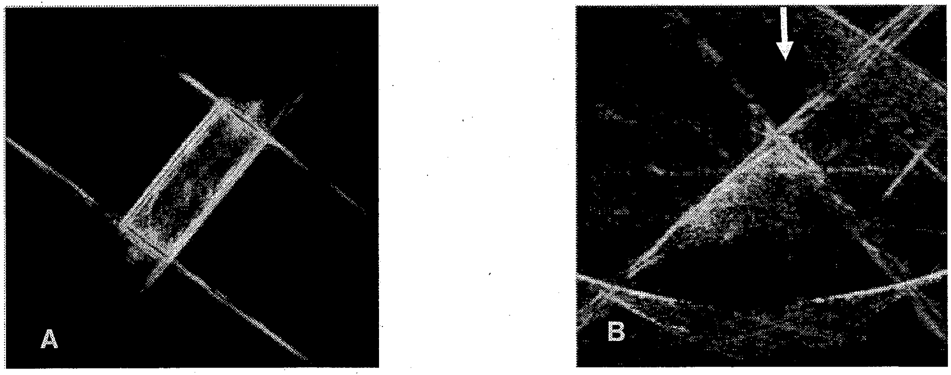

Figure 7. CSAS Images of steel cylinder. A. Monostatic image. B. Bistatic image of cylinder near edge of turntable; yellow arrow indicates source direction.

Figure 8 compares the wavenumber data, $M(k_x,k_y)$, corresponding to the monostatic and bistatic images of the steel cylinder shown in Figure 7. While the monostatic and bistatic wavenumber data are significantly different, both contain the information needed to reconstruct the cylinder image.

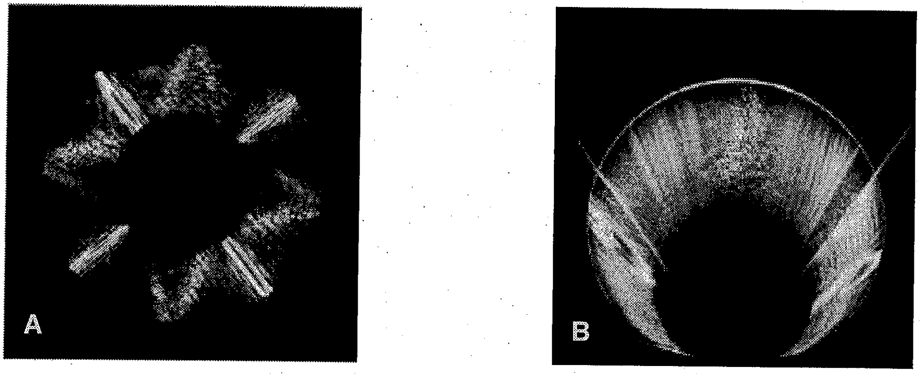

Figure 8. Monostatic and bistatic steel cylinder wavenumber data amplitudes.
A. Monostatic: ± 1000 m^{-1} scale for k_x, k_y. B. Bistatic : ± 500 m^{-1} k_x, 0-1000 m^{-1} k_y.

4 BISTATIC MOBILE PLATFORM DATA

Monostatic CSAS trials[2] were conducted at the ARL:UT Lake Travis Test Station with bottom-deployed targets and a sonar mounted on a mobile barge which circumnavigated the target field at a range of about 60 m. During these trials, bistatic data was also acquired using a fixed, omnidirectional source near the center of the target field and the receive array on the mobile barge. The transmit waveform was a 55-95 kHz LFM. For each ping, the received data includes the direct arrival from the source followed by bistatic reverberation and echoes from objects in the area. The signal processing consists of replica correlation, followed by time alignment of the direct arrivals and a bistatic time-varying gain (TVG) to compensate for one-way propagation loss from the source.

Figure 9 shows the bistatic sinogram for 30 ms of received data for 2000 pings; the 2000 pings correspond to slightly more than one full circle around the target field by the receiver. The direct arrival time is indicated by the arrow at the top of Figure 9. TVG values at ranges of 1, 10, and 20 m are shown at the bottom of Figure 9. Comparing the bistatic sinogram in Figure 9 with the corresponding monostatic sinogram[2], two major differences are observed. As expected, the bistatic sinogram "loops" or target tracks are only seen for a half cycle not a full cycle as the targets are ensonified over only 180° of aspect by the fixed source. In addition, the reverberation level is generally much lower for the bistatic data; the only significant energy in the sinogram are echoes from targets and rocks. The low reverberation is likely attributable to the shallow grazing angle, ~2° or less, between the source and the bottom in the target region for the bistatic case, compared to an angle of nearly 10° for the monostatic case.

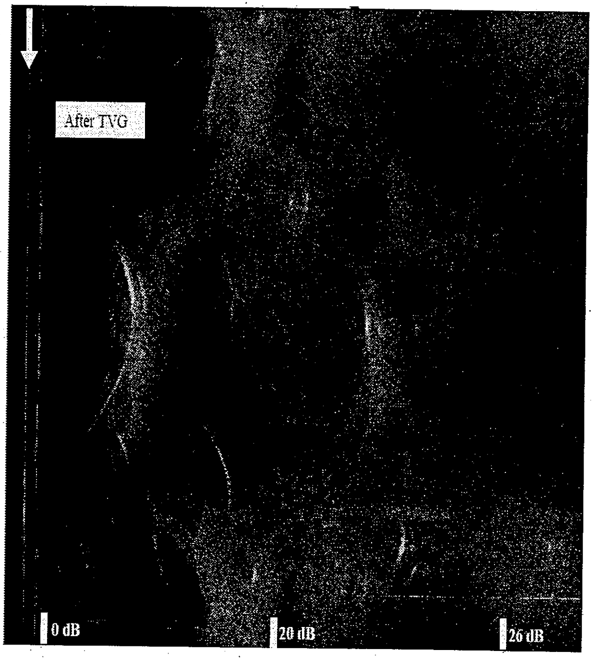

Figure 9. Bistatic Sinogram. 2000 pings, 30 ms. Data aligned to direct arrival of beacon signal. TVG at 1, 10, and 20 m ranges shown at bottom.

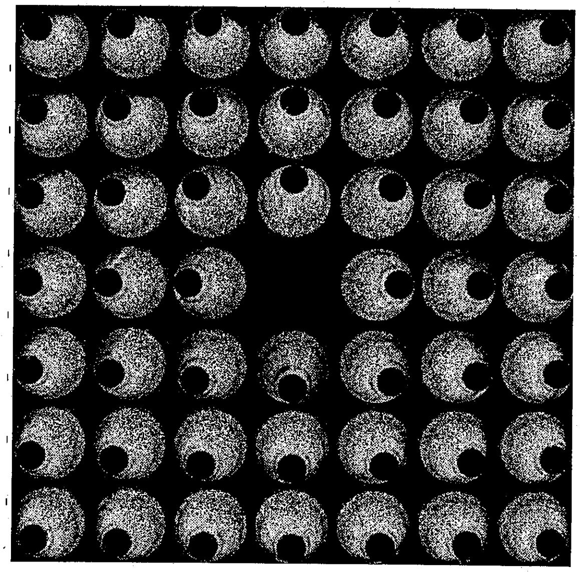

Figure 10. Bistatic wavenumber data for 49 tiles covering target region, centered on source. Each tile is spatially located in the horizontal plane; the content of each tile has dimensions of m^{-1}.

After computing the aligned bistatic sinogram in Figure 9, the focus times for the center points of 49 tiles that covered the 28 m x 28 m target region were calculated. For each tile, a refocused sinogram (with a 3° receiver beamwidth) was computed and the bistatic image processing algorithm outlined in Section 2 was implemented.

Figure 10 shows the bistatic wavenumber data amplitudes, $|M(k_x, k_y)|$, for each of the 49 tiles. Note that the source direction is different for each tile and the crescent wavenumber data shapes orient towards the source.

Figure 11 shows the resulting bistatic image for the 28 m x 28 m target region generated as a mosaic of the images from the 49 tiles. The source is located at the center of the bistatic image (0 m, 0 m) and is represented by the white star. The one complete object that can be recognized in the image is the lobster trap to the right of the source. In comparison with the monostatic image in Figure 11 of our companion paper[2], the bistatic image has a much lower reverberation level. As expected for the bistatic situation, we see only the ensonified sides of the solid objects which appear as bright lines or "flashes" in Figure 10. More importantly, all of the bright lines and spots seen in Figure 10 are parts of complete objects which can be clearly observed in the corresponding monostatic image[2]. In other words, the parts of deployed targets and scattered rocks that are ensonified by the fixed source at the center of the field are seen in the bistatic image.

Figures 12 and 13 compare 2 m x 2 m monostatic and bistatic images for two of the objects in the target field, a cylindrical mine shape and a steel cylinder, respectively. The mine shape imaged in Figure 12 is located at (1 m, 4.5 m) relative to the fixed source at (0 m, 0 m), the white star in the center of Figure 11, and is seen as a bright curved line segment above the white star in the bistatic image. The steel cylinder imaged in Figure 13 is located at (-13 m, -8.75 m) relative to the fixed source at the center of Figure 11 and is seen as a bright straight line segment near the bottom left-hand corner of the image. The center of Figure 13 is 16 m from the small source. From the expanded images shown in Figures 12 and 13, it is apparent that, for the ensonified parts of the targets which are expected to be visible, the quality of the bistatic images is at least as good as that of the monostatic images. This result gives encouragement that a bistatic operation using multiple fixed sources, as sketched in Figure 1C, will provide complete images within the central ensonified region.

5 REFERENCES

1. K.D. LePage and H. Schmidt, 'Bistatic Synthetic Aperture Imaging of Proud and Buried Targets From an AUV', IEEE J. Ocean. Eng., 27, (July 2002)
2. S.K. Mitchell, KN Scarbrough, SP Pitt, and T.S. Kooij, 'High Resolution Circular SAS with Controlled Focus', to appear in Proc. IOA, 28(5), (September 2006).

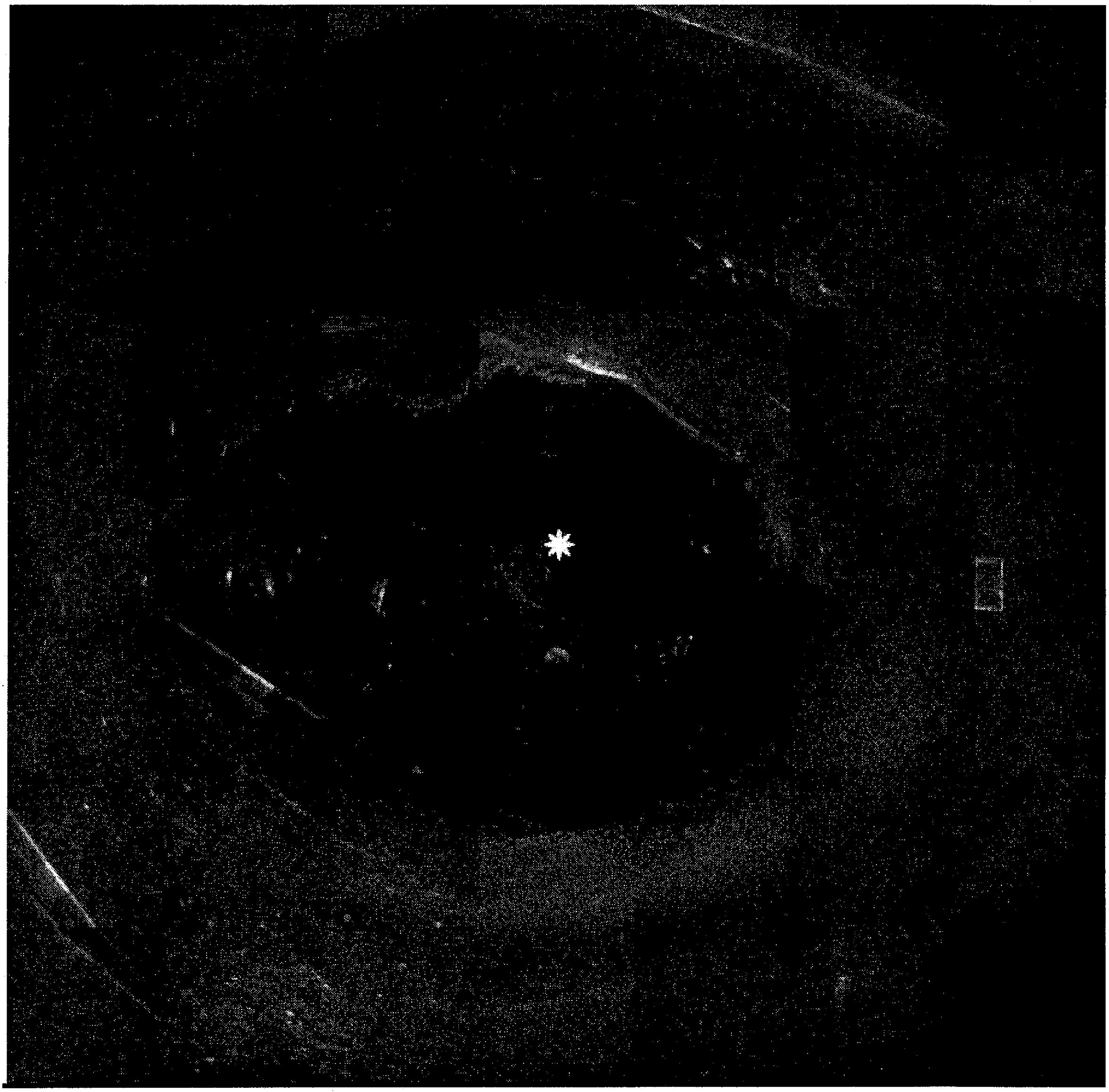

Figure 11. Bistatic image of 28 m x 28 m target region.
Fixed source at center of image (0 m, 0 m) is represented by the star shape.

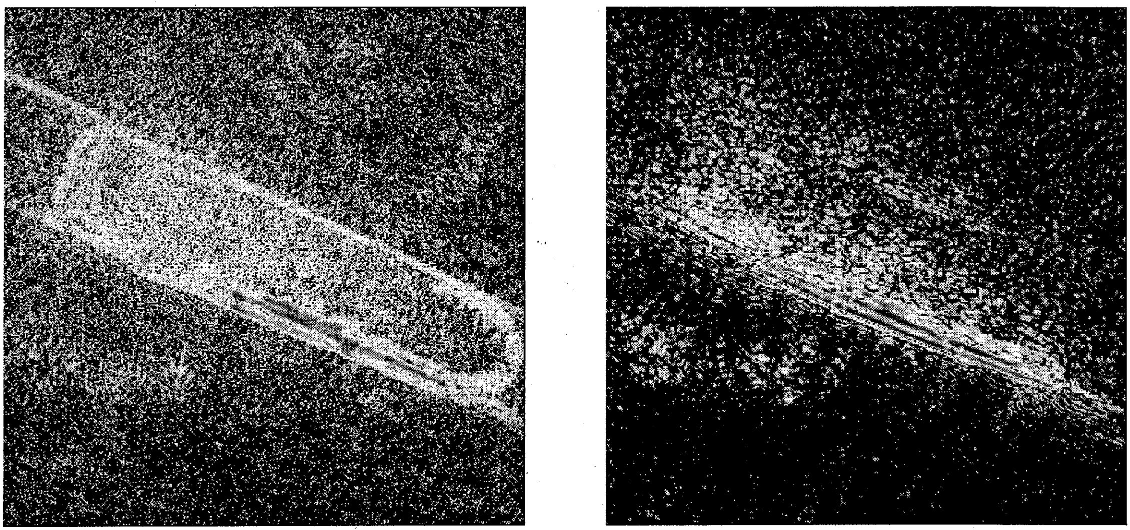

Figure 12. Monostatic and bistatic images of cylindrical mine shape located at (1 m, 4.5 m) relative to fixed source at (0 m, 0 m) in Figure 11.

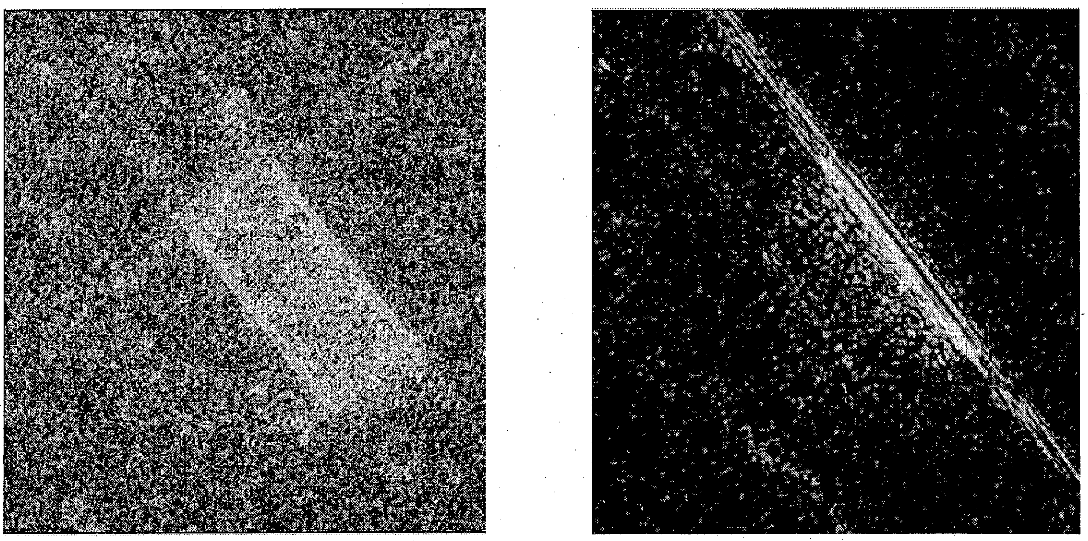

Figure 13. Monostatic and bistatic images of steel cylinder located at (-13 m, -8.75 m) relative to fixed source at (0 m, 0 m) in Figure 11.